A common four-beam geometry reveals altitude-stratified GeV pulses in canonical young pulsars

Paul K. H. Yeung *& Takayuki Saito (ICRR, UTokyo)*

Discussed with Dmitry Khangulyan & Ievgen Vovk

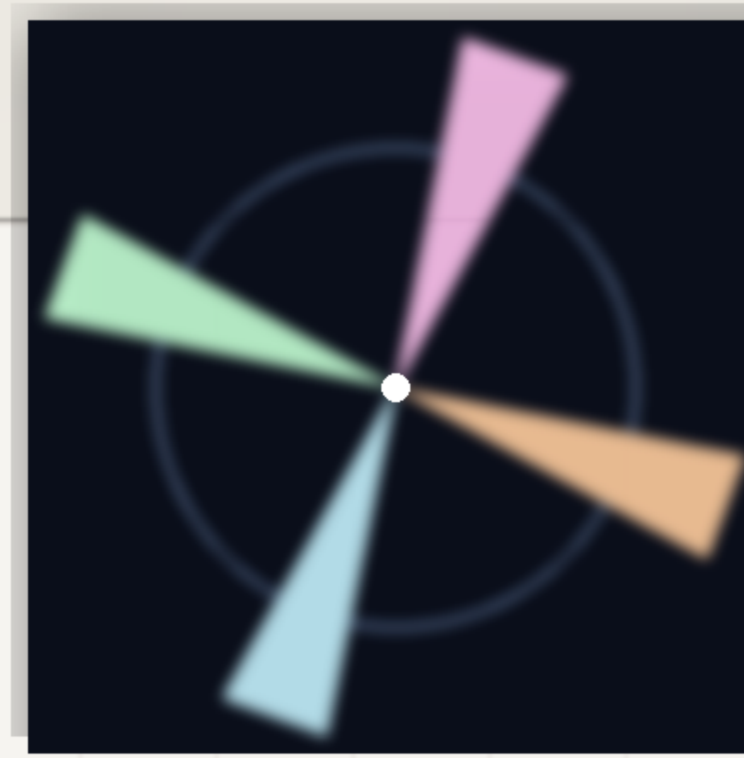

Relevant publications:
Yeung+2025, MNRAS, 541, 2053;
Yeung+2026, ApJ, 1007, 119

Why is pulsar emission periodic? *Observer's perspective*

- Pulsar is rotating rapidly
    - Equivalently, our line of sight (l.o.s.) is revolving around pulsar

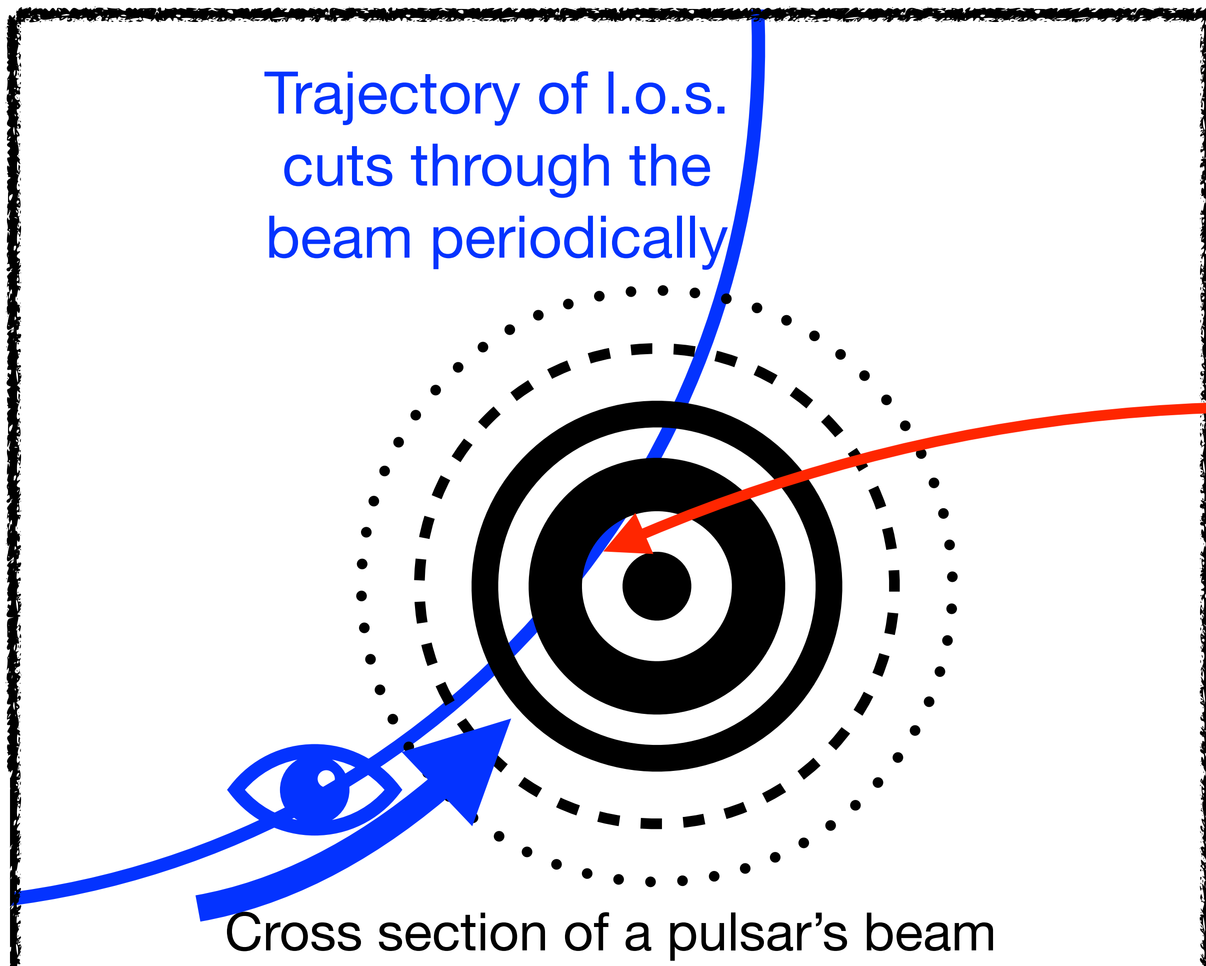

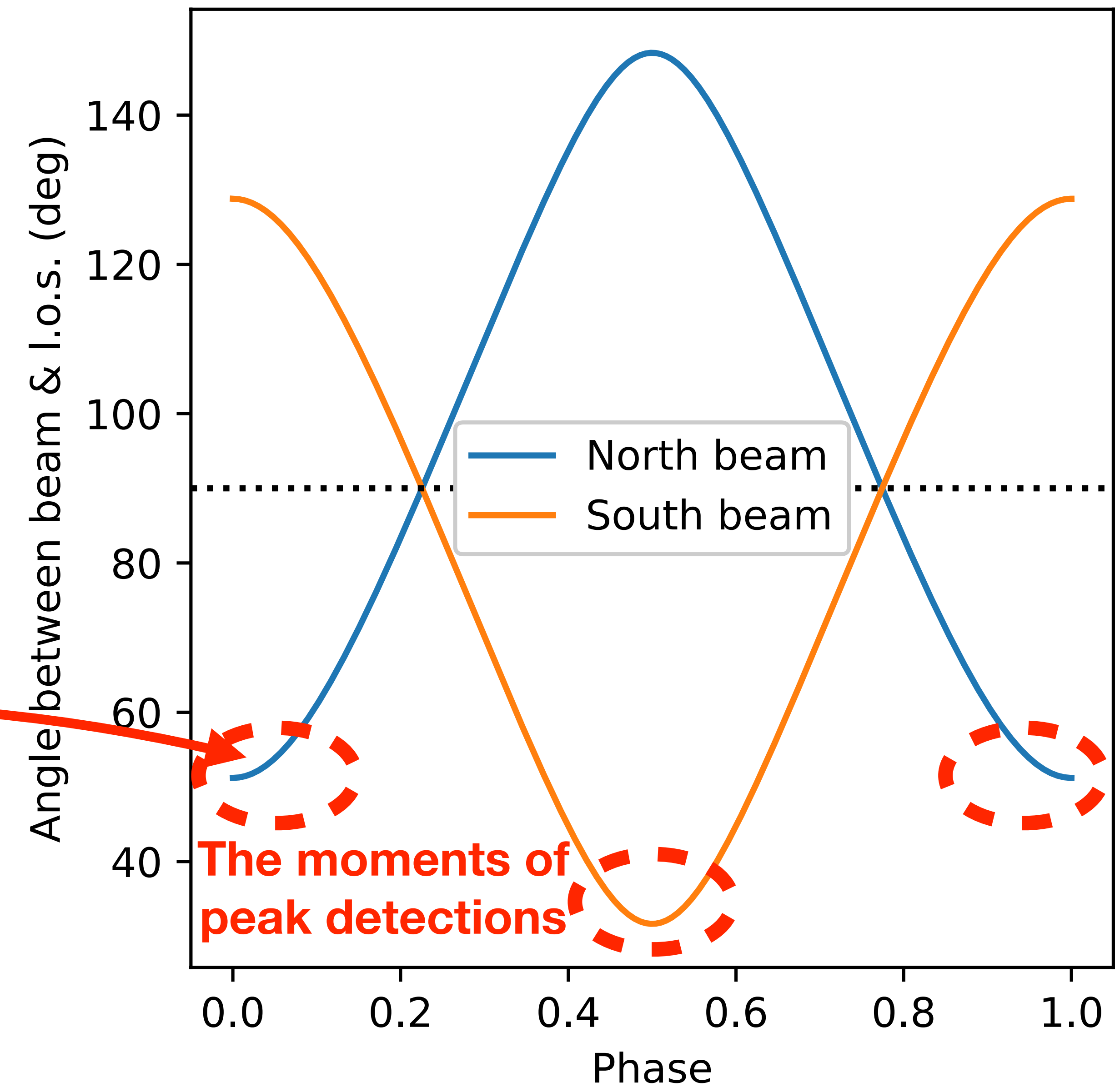

- A beam's "real" peak is *never* observable

Concepts of “motions” for pulsars

- *Aristotle (Physics):*
  “**Motion is one kind of change** – a change in place, quantity, or quality of something that already exists.”

- *Albert Einstein (Special Relativity):*
  “**Motion is the change of spatial coordinates** with time as measured in a given inertial frame.”

- In context of pulsars:
  - Kinematic Bulk Flow —> Doppler shift
  - Pattern-level “Virtual” Corotation —> Pulsation
    - Photon-emitting particles are continuously replaced in a wave-like manner

“Virtually Corotating” Emission Site

- What appears observationally “corotating”?
  ✘ Kinematic Bulk flow ❌
  ✓ Virtual motion of emissivity pattern ✔

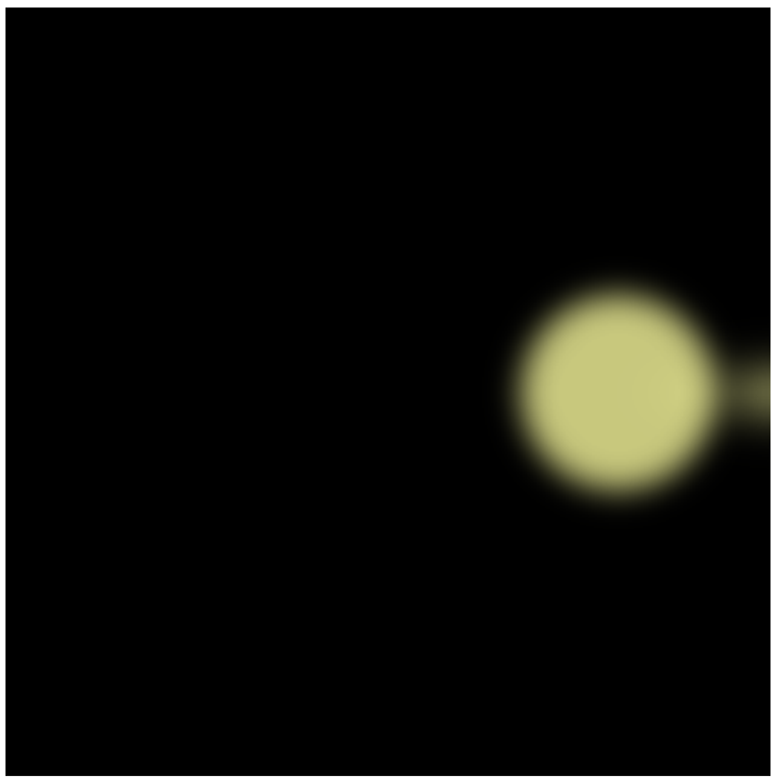

✘ A single glowing bulb rotating around a center ❌

Paul K. H. Yeung

“Kinematic Christmas Light” Analogy of Pulsar Emission Site

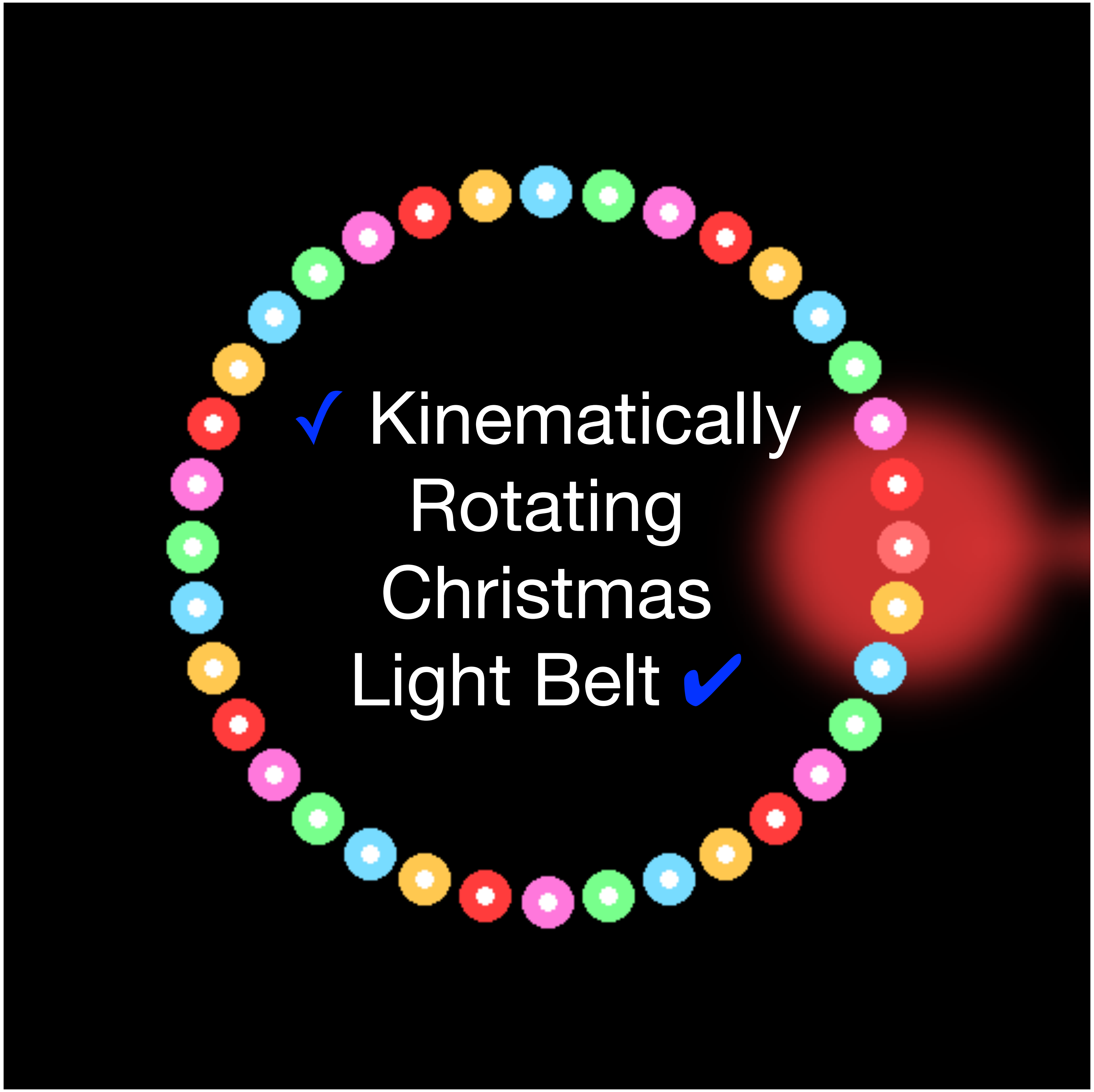

- The ON bulb is both replacing and kinematically moving.
- Only the pattern corotates; the light bulbs (plasma particles) themselves do *Not*.
- Real pulsar emission is more complex:
  - Particles also have vertical and radial drifts;
  - Each emitting particle radiates once and cools.

Paul K. H. Yeung

Emission site beyond light cylinder

‘Cold’ Ultrarelativistic Wind

Wind Current Sheet

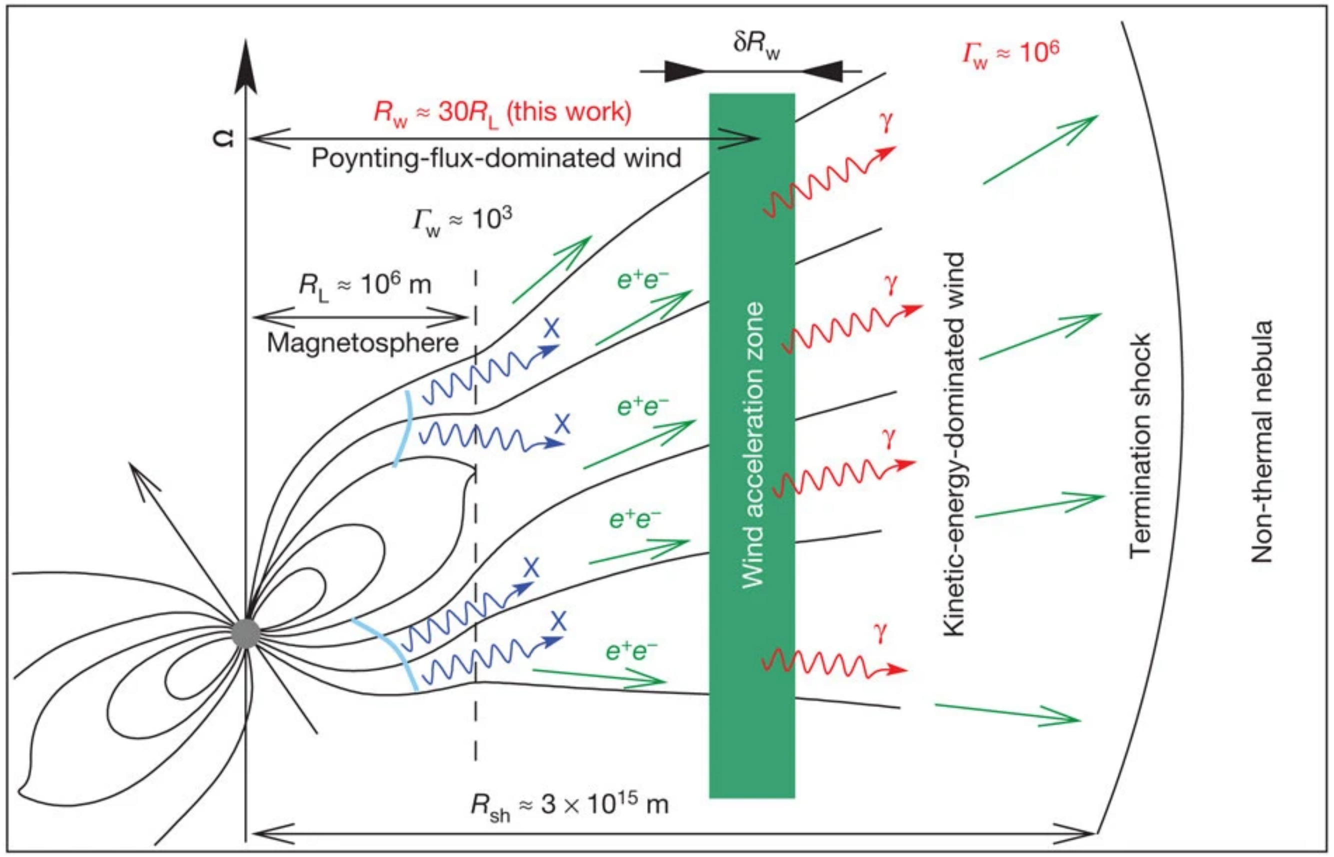

Aharonian et al. (2012, Nature)

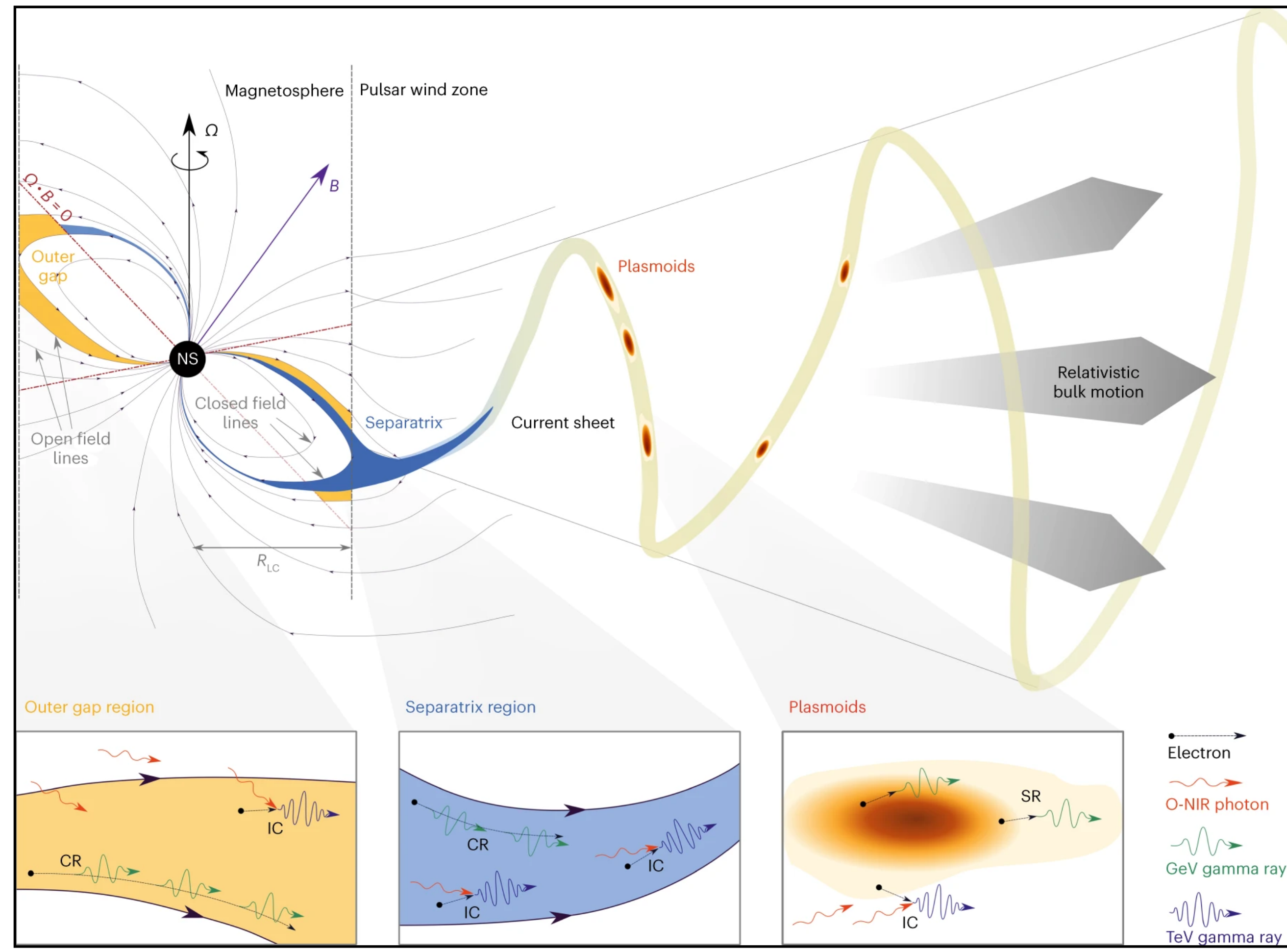

H.E.S.S. Collaboration (2023, Nature Astronomy)

No known substance can travel faster than light, but
some ‘virtual’ concepts can ‘virtually’ exceed the speed of light. ✅
pattern speed ≠ bulk speed

Purpose of mechanism-independent paradigm

- ✓ **Geometry-first** + mechanism-later ✔
- Complementary strategy to mechanism-specific modelling
- An attempt to **avoid Circular Reasoning**

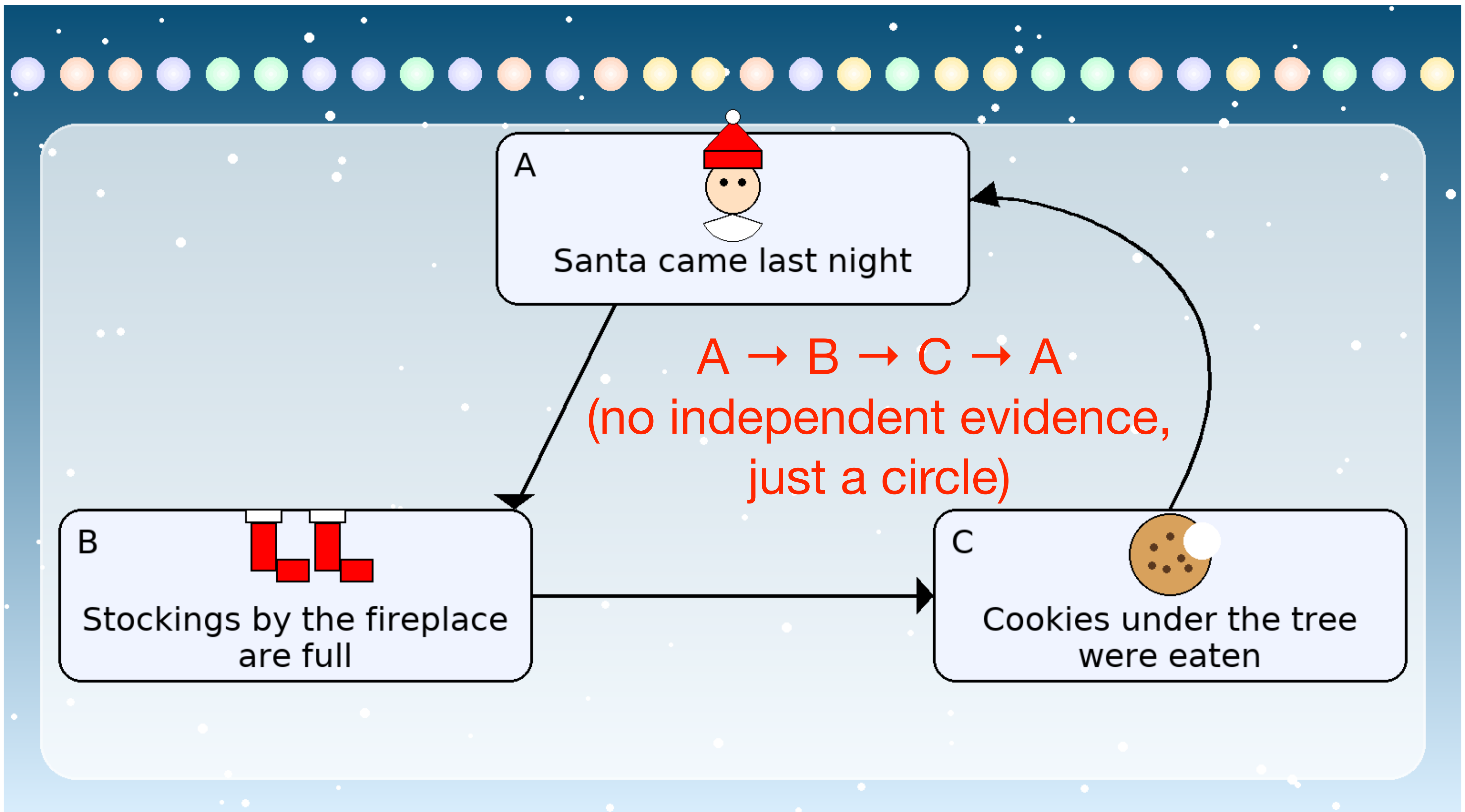

Four elements of our modelling paradigm

- Emission Geometry
- Light-Travel-Time Delay
- Phase-Dependent Doppler Shift *"Four Seasons in One Day"*
- Energy-Dependent Beam Shape

Reference Frames

- Detector frame
- Corotating frame — governing viewing angle & light-travel-time delay
- **Ever-replacing** plasma frame (bulk frame) — governing Doppler shift

Paul K. H. Yeung

Advancements of mechanism-independent modelling

v1.0 *(YKS2025, MNRAS)*	**v2.0** *(Yeung+2026, ApJ)*	
Single site, single beam per hemisphere	Double site, double beam per hemisphere	Model complexity↑
(Co-)rotating plasma	Escaping plasma	
Vertical(+Radial) extension	Point-like	Model complexity↓ / Data constraints↑
Energy-dependent geometry	Uniform geometry across energies	
Structured count-rate function	Economical beam-shape prescription	
Simultaneously fit 3 phaseograms	Simultaneously fit 4 phaseograms	

Mechanism-Independent Model v2.0

- Assume double site and double beams per hemisphere (i.e. Beam1&3 from north; Beam2&4 from south)
- Parametrise the direction of particles' drift motion as well, allowing escaping plasma.
- For each beam shape, assume a simpler function of Generalised Normal Distribution (GND). Assign amplitude a power-law energy-dependence, while assuming width & sharpness to be "locally uniform".

	Emission site location			Particles' drift motion			Beam axis	
Beam1&2	d	θB	t0	γLor1	θM	θN	θC	θQ
Beam3&4	D	φB	T0	γLor3	φM	φN	φC	φQ

	Energy-dependent beam shape			
Beam1&2	A1	η1	Ψc,1	β1
Beam3&4	A3	η3	Ψc,3	β3
	Amplitude	PL index (E-dep)	width	sharpness

$$C_i(\psi, \varepsilon) = A_i \, \varepsilon^{\eta_i} \exp\left[- \left(\frac{\psi}{\Psi_{c,i}} \right)^{\beta_i} \right]$$

$$\varepsilon \equiv E_{\mathrm{bulk}} / E_{\mathrm{det}}$$

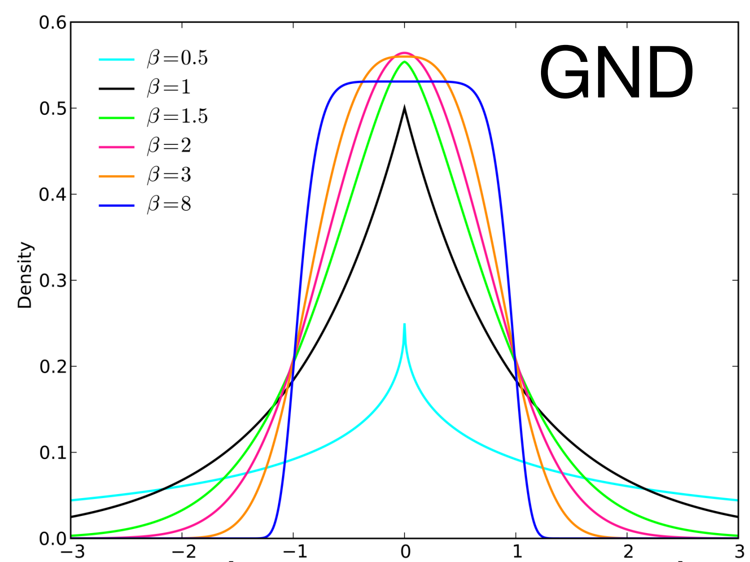

(From Wikipedia)

Paul K. H. Yeung

Light-Travel-Time Delay

- Emission site is at a separation *(d)* from pulsar center
- Times taken for North & South beams to reach us are different
- Photons' travel times vary from phase to phase
- **Time in detector frame *(t_{det})* changes non-linearly with time in pulsar frame *(t_{psr})***
- Time Delay *partially* accounts for:
    - P2–P1 phase intervals < 0.5 ;
    - Leading Wing—Trailing Wing (LW—TW) Asymmetry

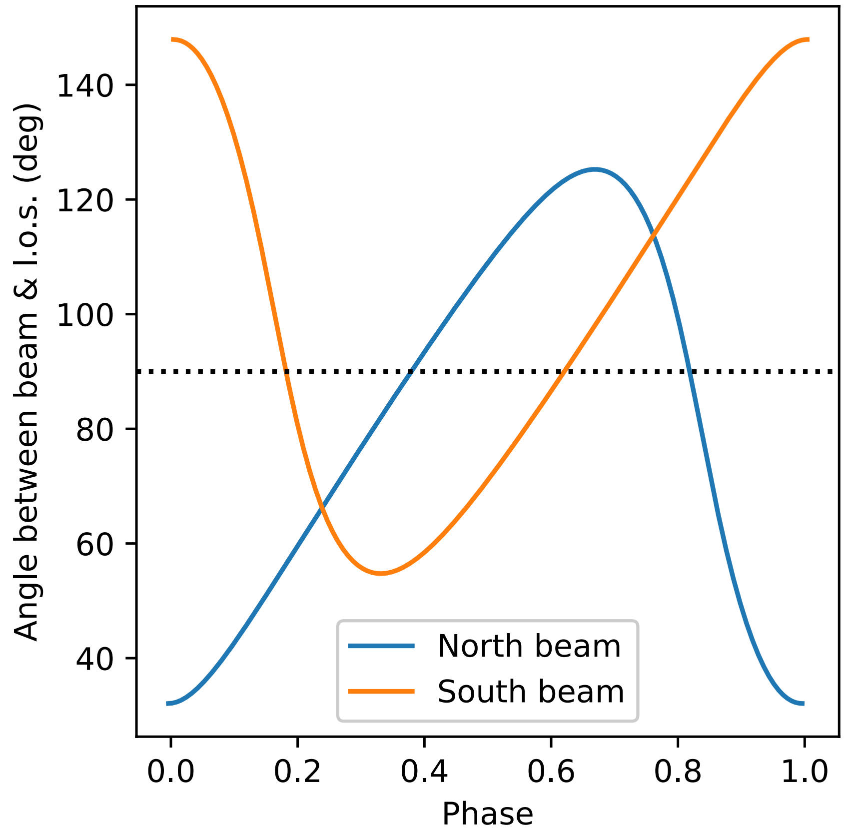

Absolute relation:
P2 phase – P1 phase =
0.5 – d*cos(θ_B)*cos(Θ_A)/R_{LC}

Phase-Dependent Doppler Shift

- Emission site moves towards us and away from us periodically
- Observed beam is redshifted & blueshifted alternately
- The level of redshift/blueshift varies from phase to phase
- **Photons with the same detected energy (E_{det}) at different phases correspond to different pre-shift energies (E_{psr})**

"Four Seasons in One Day"

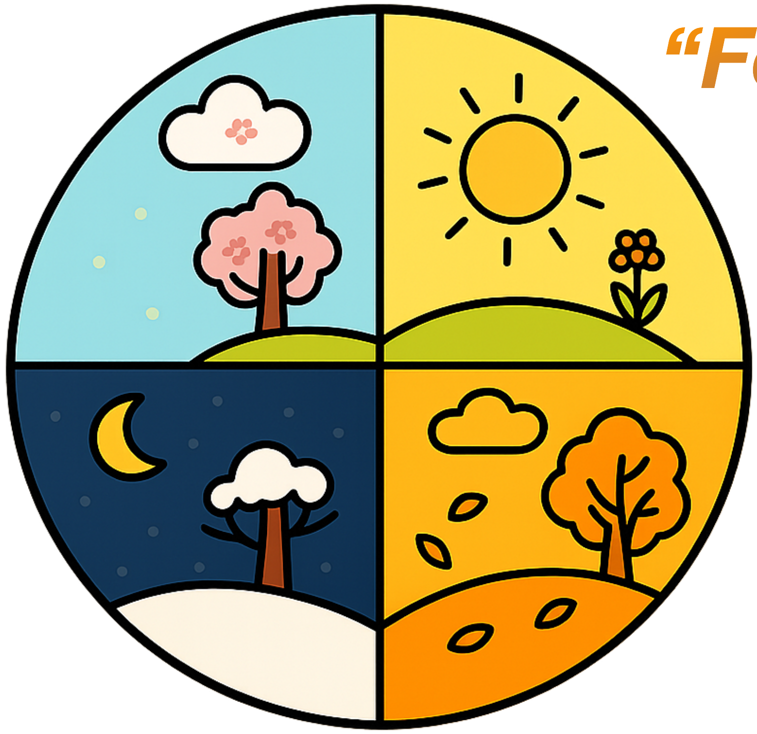

- Doppler Shift further modulates P2−P1 phase intervals & LW—TW Asymmetry

Data Samples & Scope

- 3 young pulsars: Crab, Vela & Dragonfly (<20 kyr)
  - Age trends:
    Very young Crab vs. Adolescent Vela & Dragonfly
- Below 3 GeV —> Suppress inverse-Compton
- Divide 60 MeV—3 GeV into 4 segments:
  60—150 MeV, 0.15—0.36 GeV, 0.36-0.9 GeV & 0.9—3 GeV
- Magnetosphere vs. Outflow
- Systematic errors

Paul K. H. Yeung

Crab

Spin axis—l.o.s. angle (Θ_A) = 55.7°
PWN Torus: 61°–63° *(Ng & Romani 2004)*

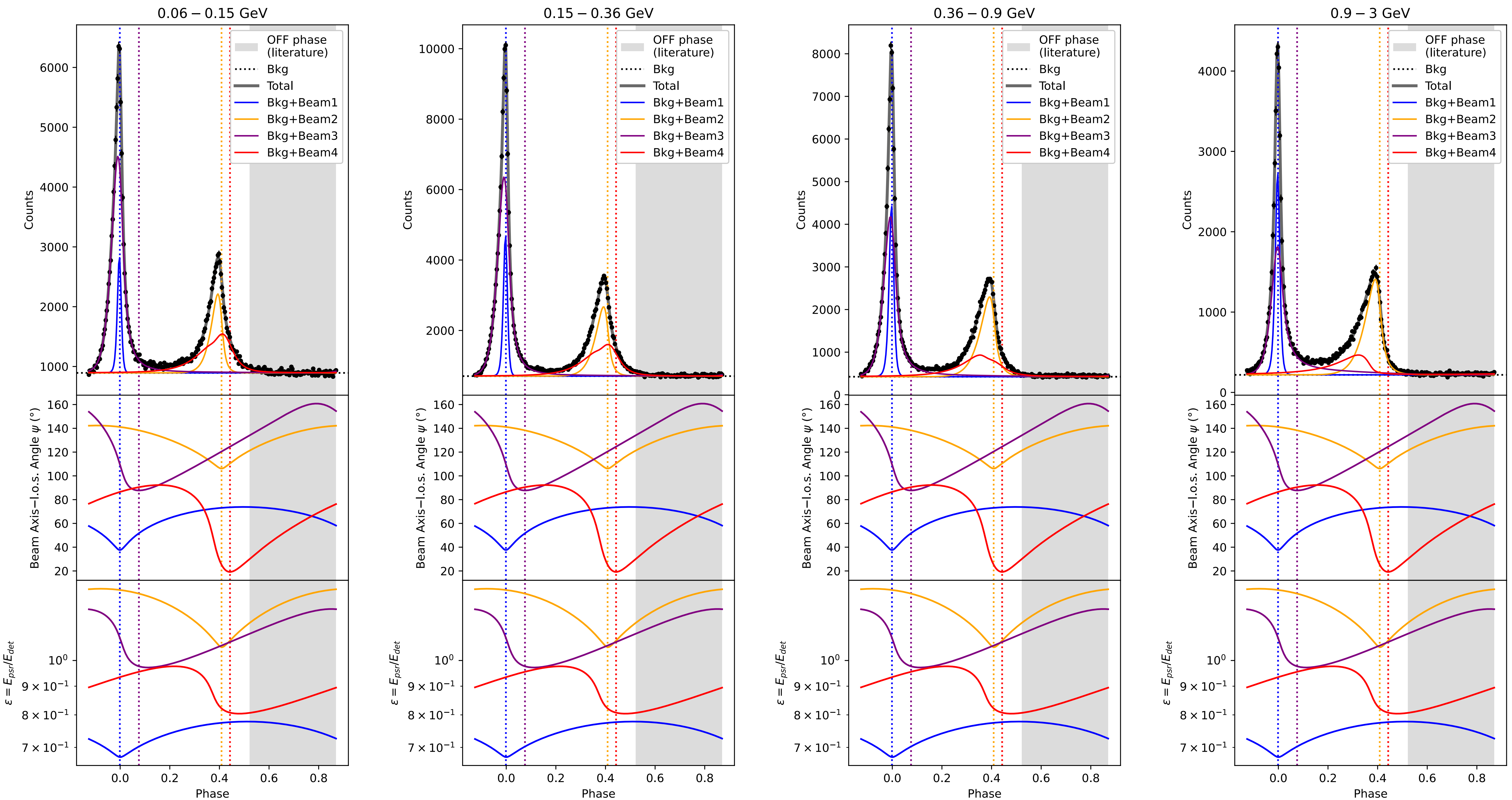

Beam3 & Beam4 are "modulation" components, accounting for bridges, overlapping with sharp primary peaks.

Credits to Jodrell Bank for monthly ephemerides

Paul K. H. Yeung

Vela

Spin axis—l.o.s. angle (Θ_A) = 54.9°
PWN Torus: 63°–64° *(Ng & Romani 2004)*

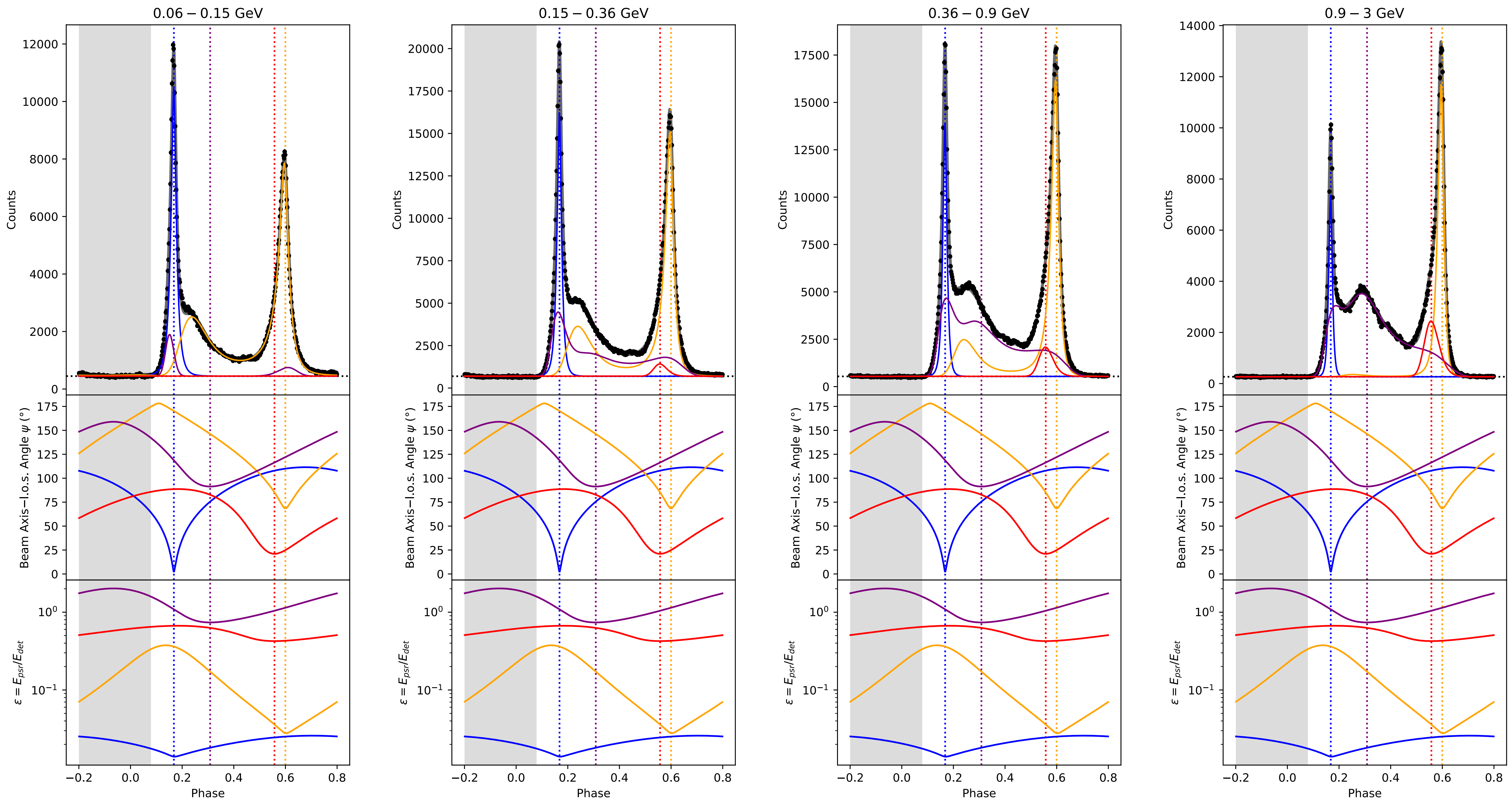

Beam3 & Beam4 are "ripple" components,
accounting for bridges, overlapping with sharp primary peaks.

Credits to Matthew Kerr for an optimised ephemeris

Paul K. H. Yeung

Dragonfly

Spin axis—l.o.s. angle (Θ_A) = 80.9°
PWN Torus: 85°—88° *(Van Etten et al. 2008; Jin et al. 2023)*

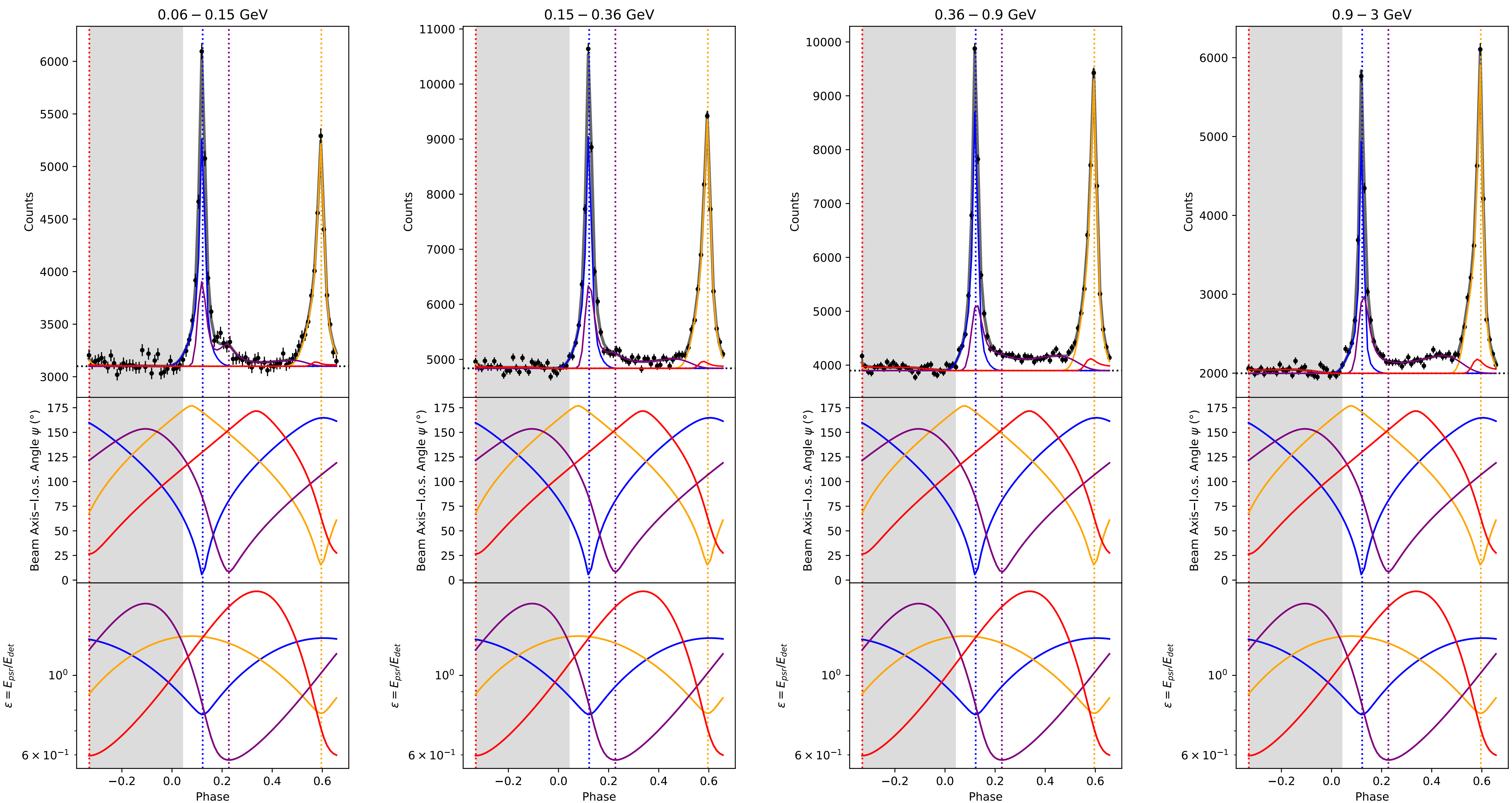

Beam3 & Beam4 are "ripple" components,
accounting for bridges, overlapping with sharp primary peaks.

Credits to Fermi 3PC for an event list

Magic of Doppler Boost

- Away from the beam axis, the count rate generally drops.
- This angle-dependent decrement could be countered/overcome by energy-dependent increment.
- The interplay between energy-dependent beam shape & Doppler Boost could lead to an **extensive tail** or even **sub-spikes** of a pulse component.
- This effect is more conspicuous for Beams3—4.

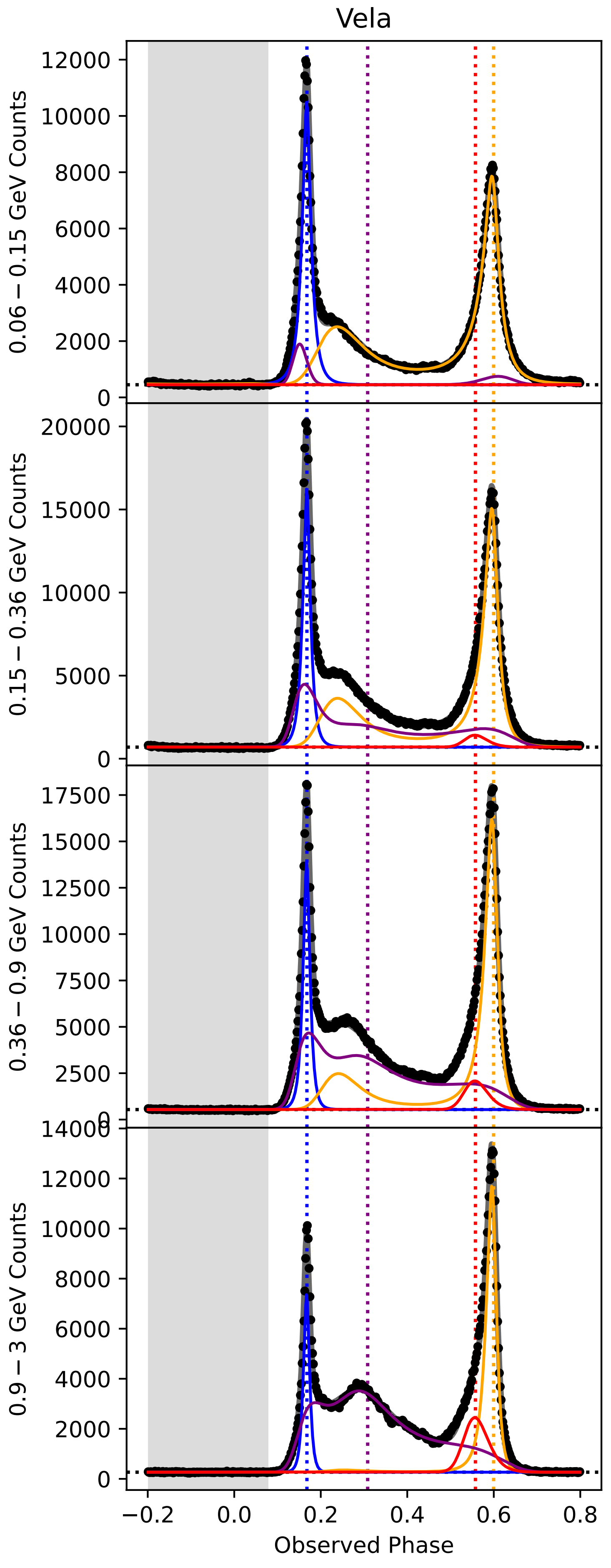

Paul K. H. Yeung

Schematic Diagrams

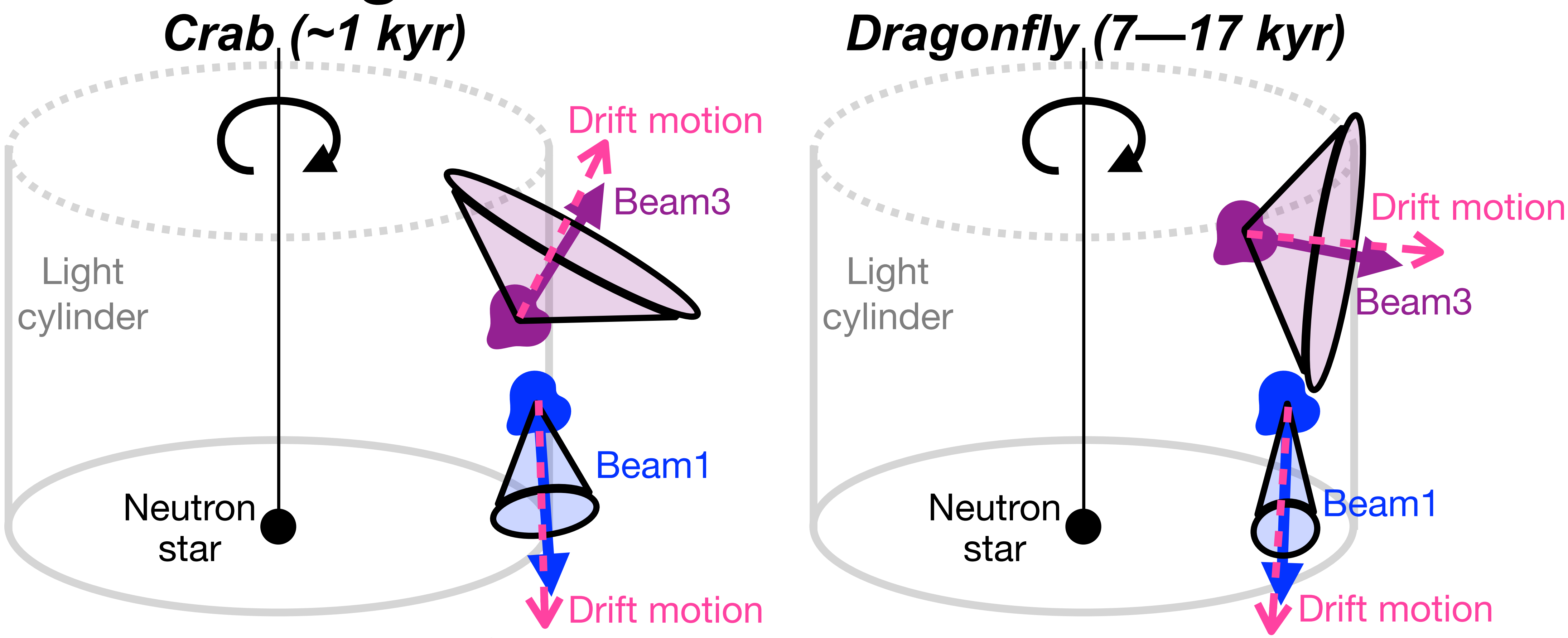

Only the northern hemisphere is shown. The southern configuration is obtained by inverting all coordinates through the origin.

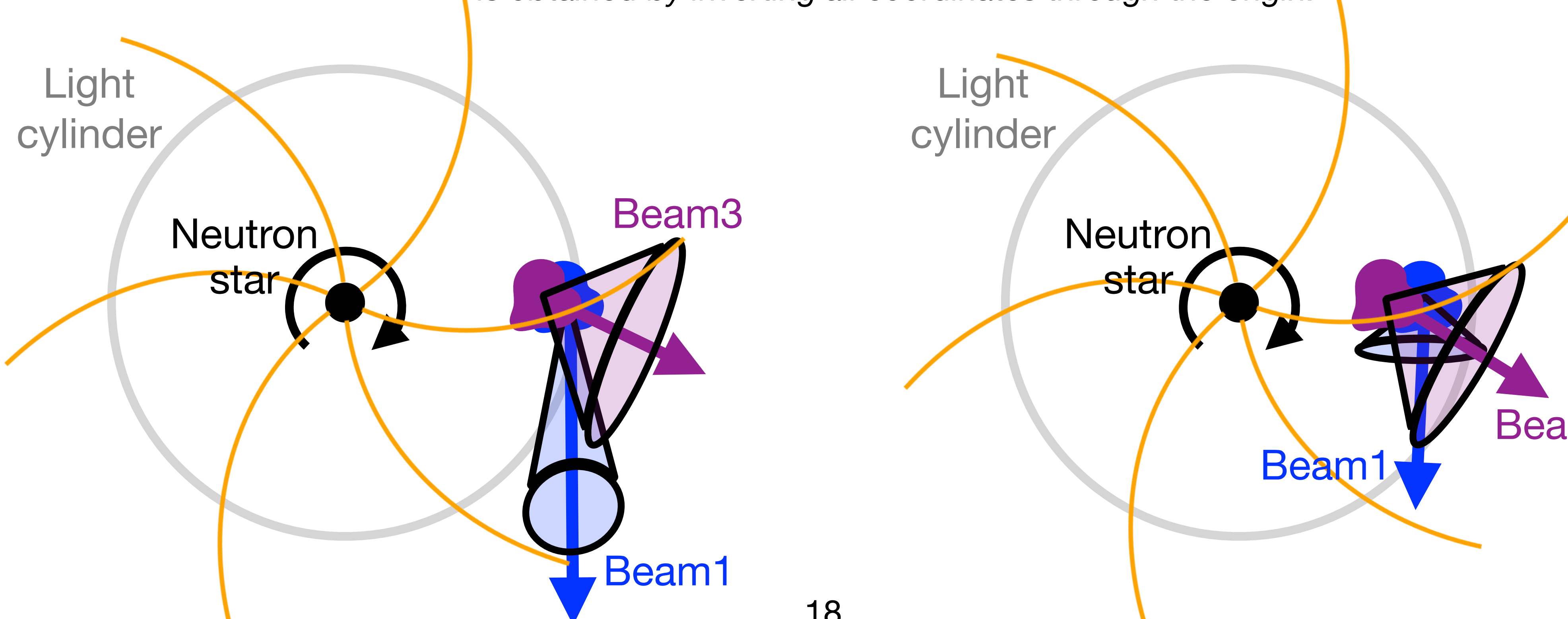

Definitions of Parameters

Spin axis — l.o.s.		**ΘA**	The angle between our l.o.s. and the pulsar's rotational axis.
Beam1 & Beam2	**Emission site location**	**d*sin(θB)**	The average radial separation of the emission site from the pulsar centre.
		d*cos(θB)	The average vertical separation of the emission site from the pulsar centre.
		t0	The phase (in the detector frame) corresponding to the moment when the Beam1's emission site is at its closest approach to our l.o.s.
	Bulk motion (related to Doppler Shift)	**γLor1**	The average Lorentz factor of the collective motion of the emission site.
		θM	The bulk velocity vector's zenith angle measured from the rotational axis.
		θN	The azimuthal angle by which the bulk velocity vector is ahead of the emission site.
	Beam axis	**θC**	The beam axis's zenith angle measured from the rotational axis.
		θQ	The azimuthal angle by which the beam axis is ahead of the emission site.
Beam3 & Beam4	**Emission site location**	**D*sin(ϕB)**	The average radial separation of the emission site from the pulsar centre.
		D*cos(ϕB)	The average vertical separation of the emission site from the pulsar centre.
		T0	The phase (in the detector frame) corresponding to the moment when the Beam3's emission site is at its closest approach to our l.o.s.
	Bulk motion (related to Doppler Shift)	**γLor3**	The average Lorentz factor of the collective motion of the emission site.
		ϕM	The bulk velocity vector's zenith angle measured from the rotational axis.
		ϕN	The azimuthal angle by which the bulk velocity vector is ahead of the emission site.
	Beam axis	**ϕC**	The beam axis's zenith angle measured from the rotational axis.
		ϕQ	The azimuthal angle by which the beam axis is ahead of the emission site.

Clarifications: Magnetic poles are Not parametrised. Rotational axis = Zenith.

Magnetosphere (Beams 1–2) & Age Trends

- Beams 1–2 originate radially close to the light-cylinder wall, suggesting emission from the **outermost magnetospheric zones**.

- θN ≃ 80°−100° ==> **Bulk motions remain nearly tangential** and strongly tied to quasi-rigidly co-rotating field-line bundles near the last closed field lines.

- θM declines with age ==> Flows roughly follow **field lines** whose **tangents in older systems progressively align with the equatorial plane.**

Outflow (Beams 3–4) & Age Trends

- Beams 3–4 arise at smaller cylindrical radii but higher vertical altitudes, implying a **rotation-decoupled outflow**.
- **The vertical migration of Beams 3–4 traces the weakening magnetic confinement with age:**
  - Very young Crab's high magnetization and strong field-tension keep the outflow zones still entangled with the outer magnetosphere;
  - Adolescent Vela and Dragonfly (with reduced magnetisation & reduced field-tension) allow vertical inflation of the emission zone and and clearer outflow-dominated geometry.
- Two sites at one hemisphere are nearly co-longitudinal: $|\Delta\phi_{site}| \lesssim 12°$.

Toroidal Magnetic Field

- **Hoop stress of the toroidal magnetic field** naturally narrows high-latitude outflows toward the spin axis, giving smaller radial separations at higher altitudes.

- Two beam axes at one hemisphere are azimuthally (i.e. longitudinally) separated by $\Delta\phi_{beam} \simeq 40°–65°$.
    - Outflow-transition layer is swept back by plasma inertia and a growing toroidal field component.

Mildly Relativistic & Highly Relativistic Bulk Flow

- Fitted γ_{Lor} should be regarded as an **effective** Lorentz factor along the beam direction.

- In general, the pulse-emitting plasma is **mildly relativistic** ($1.03 \lesssim \gamma_{Lor} \lesssim 1.5$) for all three pulsars.

  - ==> Pulsed emissions are likely associated with magnetosphere & outflow-transition layer.

- Relatively large bulk Lorentz factor ($\gamma_{Lor} > 10$) is inferred for primary pair in Vela

  - ==> Consistent with particularly fast flows in the outer magnetosphere

  - Coincidently, primary site of Vela is around the edge of the light cylinder ($d^* \sin\theta_B \simeq 1.0\ R_{LC}$)

- True flow in the transition layer may well contain ultra-relativistic components, but turbulence, pitch-angle spreads and the extended current-sheet geometry can dilute the net beaming towards the observer

Beam–Motion Alignment

- Angular separation between a beam axis and a bulk flow direction are computed using the scalar product formula.

	Crab	**Vela**	**Dragonfly**
$\Delta\theta$ (°)	3.9	23.9	1.0
$\Delta\phi$ (°)	10.3	2.6	2.1

- Observed γ-ray beams trace bulk flows, rather than being strongly smeared by large pitch angles or long propagation distances.
- Along beam axis: Intrinsically brightest emission pattern.
- Along bulk-flow direction: Maximal Doppler boosting.

Speculations on magnetic-field configuration and radiation mechanisms

- **Beams 1–2** are rooted near the last closed field lines and following extended trajectories that graze the light-cylinder boundary
==> Compatible with **curvature radiation**
(e.g. outer gap/slot gap)

- **Beams 3–4** emerge at larger |z| in regions where the magnetic field is predominantly toroidal and the flow has entered the wind zone
==> Suited to **synchrotron radiation**
(e.g. wind current sheet)

- Inverse-Compton is very minor below 3 GeV

Clarifications on assumptions

- **North–south symmetry: local, not global ($r \lesssim R_{LC}$)**
    - PWN/SNR asymmetries occur on >> R_{LC} scales
      → Not contradicting our **near-source** symmetry
- **Circular beam "kernel" in the bulk frame (minimal assumption)**
    - Enables stable component decomposition;
    - Misaligned beam axes + Time delay + Doppler shift
      → **effective** hemispheric asymmetry in the observer frame

Paul K. H. Yeung

Additional Information *(Yeung+2026, ApJ)*

Table 1: Geometric and kinematic parameters of the four-beam configurations. Quoted uncertainties are the quadratic sum of statistical and systematic errors from the band-edge tests described in the Supplementary Material.

	Crab	Vela	Dragonfly
$\Theta_{\rm A}$ (°)	55.7 ± 5.6	54.9 ± 0.6	80.9 ± 1.4
Beams 1 and 2			
$d \sin\theta_{\rm B}/R_{\rm LC}$	0.96 ± 0.13	1.01 ± 0.01	0.74 ± 0.01
$d \cos\theta_{\rm B}/R_{\rm LC}$	0.50 ± 0.05	0.37 ± 0.01	0.53 ± 0.07
t_0 (phase)	0.122 ± 0.005	0.286 ± 0.001	0.260 ± 0.001
$\gamma_{\rm Lor1}$	1.12 ± 0.07	37.3 ± 0.4	1.032 ± 0.001
$\theta_{\rm M}$ (°)	165.7 ± 0.9	146.9 ± 0.4	97.1 ± 0.5
$\theta_{\rm N}$ (°)	87.3 ± 2.7	82.6 ± 0.1	94.3 ± 0.7
$\theta_{\rm C}$ (°)	161.9 ± 1.0	123.3 ± 0.6	96.1 ± 0.3
$\theta_{\rm Q}$ (°)	90.2 ± 1.8	87.9 ± 0.1	94.5 ± 0.7
Beams 3 and 4			
$D \sin\phi_{\rm B}/R_{\rm LC}$	0.92 ± 0.08	0.60 ± 0.01	0.64 ± 0.02
$D \cos\phi_{\rm B}/R_{\rm LC}$	0.74 ± 0.15	1.37 ± 0.01	1.14 ± 0.18
T_0 (phase)	0.137 ± 0.001	0.395 ± 0.005	0.304 ± 0.003
$\gamma_{\rm Lor3}$	1.027 ± 0.048	1.43 ± 0.01	1.153 ± 0.007
$\phi_{\rm M}$ (°)	34.9 ± 1.5	31.2 ± 0.6	105.3 ± 5.5
$\phi_{\rm N}$ (°)	9.4 ± 11.1	36.8 ± 0.6	33.7 ± 0.8
$\phi_{\rm C}$ (°)	36.5 ± 1.4	33.8 ± 0.6	107.4 ± 5.4
$\phi_{\rm Q}$ (°)	26.9 ± 9.3	37.0 ± 0.6	34.0 ± 0.8
Additional geometrical properties[a]			
$\Delta\theta^{\rm b}$ (°)	3.9	23.9	1.0
$\Delta\phi^{\rm b}$ (°)	10.3	2.6	2.1
$\Delta\varphi_{\rm site}{}^{\rm c}$ (°)	−4.4	−12.4	4.9
$\Delta\varphi_{\rm beam}{}^{\rm c}$ (°)	58.9	38.5	65.4

Notes. [a] These additional properties are computed by substituting some iterated parameters into specific equations.

[b] Angular separation between a beam axis and a bulk flow direction ($\Delta\theta$ for Beams 1 and 2, $\Delta\phi$ for Beams 3 and 4). These are computed using the scalar product formula.

[c] Azimuthal separation between the primary and secondary emission sites ($\Delta\varphi_{\rm site}$), and azimuthal separation between the corresponding beam axes ($\Delta\varphi_{\rm beam}$). Relevant formulae are shown in Supplementary Material.

Table 2: Energy-dependent beam-shape parameters for the Crab, Vela and Dragonfly pulsars. Best-fitting parameters of the generalised-normal-distribution (GND) beam shapes for Beams 1–2 and Beams 3–4 in each of the four energy bands used in the analysis (60–150 MeV, 150–360 MeV, 360–900 MeV, 0.9–3 GeV). Statistical uncertainties on these parameters are below 1% and are therefore omitted for clarity.

	Crab				Vela				Dragonfly			
$E_{\rm det}$ (GeV)	0.06 – 0.15	0.15 – 0.36	0.36 – 0.90	0.90 – 3.0	0.06 – 0.15	0.15 – 0.36	0.36 – 0.90	0.90 – 3.0	0.06 – 0.15	0.15 – 0.36	0.36 – 0.90	0.90 – 3.0
Beams 1 and 2												
$\log_{10} A_1$	83.0	74.5	60.1	60.3	28.4	36.8	43.4	56.1	59.2	67.6	81.2	118.6
η_1	340.2	299.2	237.8	238.1	13.2	17.5	21.2	28.1	509.0	583.0	706.0	1049.0
$\Psi_{c,1}$ (°)	2.2	2.2	2.6	2.5	18.6	16.3	15.0	13.4	7.0	6.7	6.0	5.0
β_1	1.38	1.35	1.34	1.33	1.73	1.75	1.77	1.81	1.88	1.89	1.89	1.90
Beams 3 and 4												
$\log_{10} A_3$	10.9	11.0	9.5	6.4	151.6	153.4	145.9	138.4	128.9	111.3	78.8	78.7
η_3	77.4	77.8	68.5	54.0	478.0	389.0	369.0	349.2	532.0	458.0	321.2	321.9
$\Psi_{c,3}$ (°)	10.1	10.4	13.9	30.2	8.7	5.4	5.6	5.8	5.7	6.4	7.7	7.8
β_3	1.33	1.35	1.45	1.94	2.27	1.92	1.93	1.93	1.96	1.97	1.98	2.00
$C_{\rm bkg}$	893.0	704.0	424.0	218.5	449.0	695.0	539.0	266.6	3100	4840	3900	1998

Doppler formula

$$\begin{cases} \varepsilon = \dfrac{E_{\rm bulk}}{E_{\rm det}} = \dfrac{1}{\gamma_{\rm Lor}\left(1 - \beta\cos\psi_{\rm vel}\right)} \\ \cos\psi_{\rm vel} = -\sin\Theta_{\rm A}\,\cos\!\left(\theta_{\rm N} + 2\pi\varphi\right)\,\sin\theta_{\rm M} \\ \qquad\qquad + \cos\Theta_{\rm A}\,\cos\theta_{\rm M} \end{cases}, \qquad (1)$$

where $\gamma_{\rm Lor}$ is the corresponding Lorentz factor, $\psi_{\rm vel}$ is the angle between $\boldsymbol{v}$ and the line of sight, and φ denotes the pulsar's rotational angle.

Summary & Outlook

- Our geometry-first paradigm:
  - organises Crab, Vela and Dragonfly within a common four-beam framework;
  - makes testable predictions for other young pulsars / future MeV–PeV observations;
  - remains mechanism-independent: different models can be confronted within the same geometric + Doppler framework.

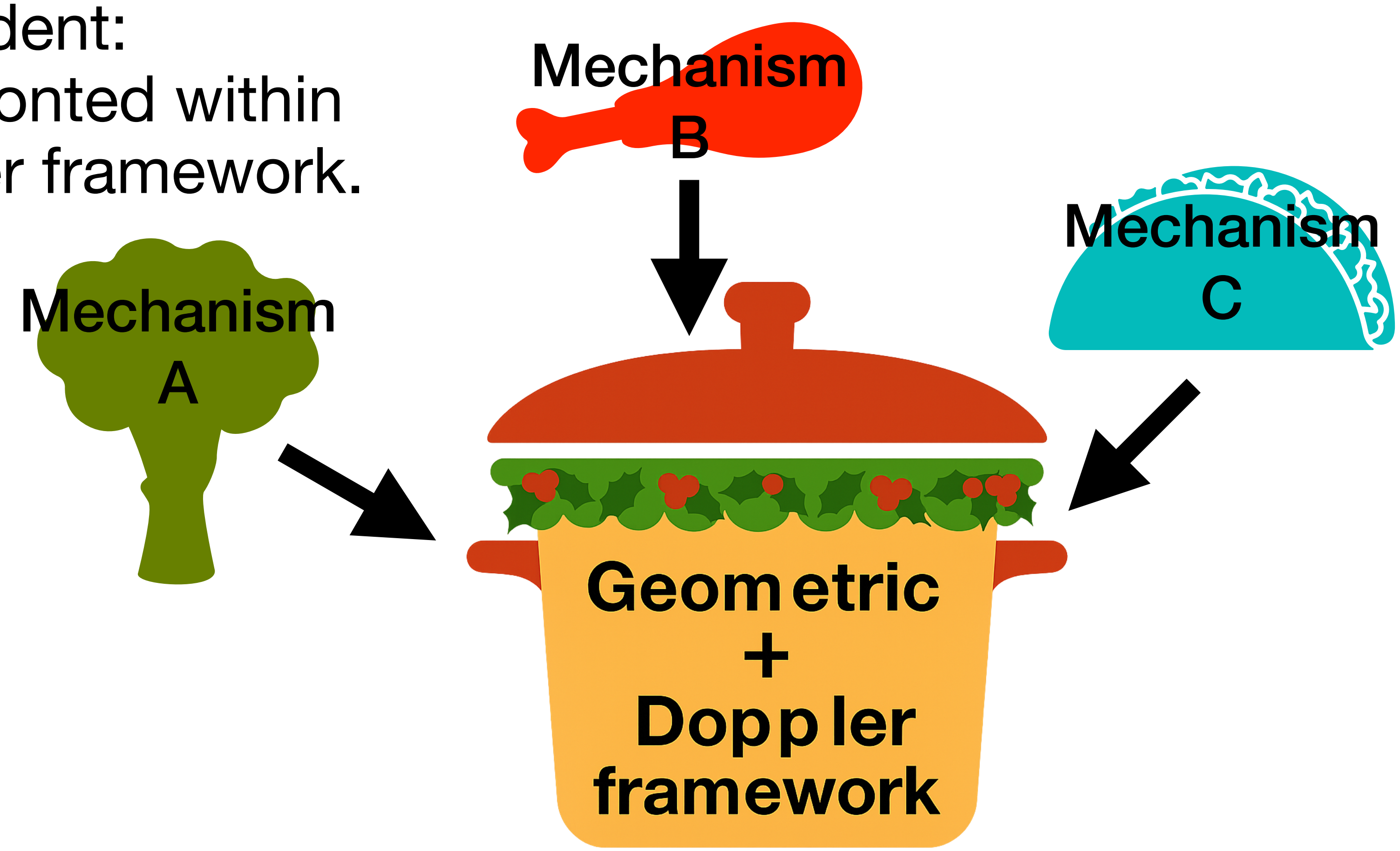

- Outlook:
  - Four-beam geometry is judged *not* by how elegant it looks, but by how well it predicts and organises γ-ray data.


Don't forget about pulsars
during Christmas